Antimicrobial peptide-loaded decellularized placental sponge as an excellent antibacterial skin substitute against XDR clinical isolates

Hatef Ghasemi Hamidabadi
Mazandaran University of Medical Sciences
Sanaz Alizadeh
Iran University of Medical Sciences
Leila Mahboobi
Iran University of Medical Sciences
Zahra Khosrowpour
Iran University of Medical Sciences
Maryam Nazm Bojnordi
Mazandaran University of Medical Sciences
Zahra Aliakbar Ahovan
Shahid Beheshti University of Medical Sciences
Majid Malekzadeh Shafaroudi
Mazandaran University of Medical Sciences
Maria Zahiri (maria_zahiri@yahoo.com)
Bushehr University of Medical Sciences
Narendra Pal Singh Chauhan
Bhupal Nobles' University
Mazaher Gholipourmalekabadi
Iran University of Medical Sciences

Research Article

Keywords: Skin substitute, antibacterial wound dressing, resistant bacteria, post-wound infection, AMP

Posted Date: October 27th, 2022

DOI: https://doi.org/10.21203/rs.3.rs-2188295/v1

Additional Declarations: No competing interests reported.

Version of Record: A version of this preprint was published at Amino Acids on June 14th, 2023. See the published version at https://doi.org/10.1007/s00726-023-03277-2.

Abstract

Post-wound infections have remained a serious threat to society and healthcare worldwide. Attempts are still being made to develop an ideal antibacterial wound dressing with high wound healing potential and strong antibacterial activity against extensively drug-resistant bacteria (XDR). In this study, a biological-based sponge was made from decellularized human placenta (DPS), then loaded with different concentrations (0, 16 µg/mL, 32 µg/mL, 64µg/mL) of an antimicrobial peptide (AMP, CM11) to optimize an ideal antibacterial wound dressing. The decellularization of DPS was confirmed by histological evaluations and DNA content assay. The DPS loaded with different contents of antimicrobial peptides (AMPs) showed uniform morphology under a scanning electron microscope (SEM) and cytobiocompatibility for human adipose tissue-derived mesenchymal stem cells. Antibacterial assays indicated that the DPS/AMPs had antibacterial behavior against both standard strain and XDR *Acinetobacter baumannii* in a dose-dependent manner, as DPS loaded with 64µg/mL showed the highest bacterial growth inhibition zone and elimination of bacteria under SEM than DPS alone and DPS loaded with 16 µg/mL, 32 µg/mL AMP concentrations. The subcutaneous implantation of all constructs in the animal model demonstrated no sign of acute immune system reaction and graft rejection, indicating *in vivo* biocompatibility of the scaffolds. Our findings suggest the DPS loaded with 64 µg/mL as an excellent antibacterial skin substitute, and now promises to proceed with pre-clinical and clinical investigations.

1. Introduction

Skin wound infection is one of the most important impediments to proper tissue healing. Colonization of the wound by opportunistic and pathogenic bacteria causes obstruction of blood vessels, a prolonged period of inflammation, delay in wound healing, and contributes to the chronic state. Additionally, multidrug resistance (MDR) in clinical isolates is one of the most difficult problems that is considered a major public health threat(Rezaei et al., 2020). Local antibiotic therapy is currently the most effective technique for treating infectious diseases. Antibiotic drug abuse has increased the incidence of MDR bacteria as a global concern(Moosazadeh Moghaddam et al., 2018a). Therefore, attempts have been made to develop new antibiotics or antibacterial agents such as antibacterial metals, antibacterial macromolecules, and antimicrobial peptides (AMPs) with minimal risk of bacterial drug resistance, as an alternative to antibiotic therapy(Ahovan et al., 2020). AMPs are known as short and water-soluble host defense peptides to exist in different kinds of microorganisms in human tissues. Due to immunomodulatory properties and direct action against bacteria, AMP act as a viable alternative to antibiotics in the post-antibiotic era. (Mahlapuu et al., 2016). The CM11 is an amphipathic cationic peptide that acts as a cell-permeable agent. There is an electrostatic interaction between positive charges of AMP with polyanionic substances on the surface of the bacterial cell membrane, such as teichoic acid in Gram-positive bacteria and lipopolysaccharide in Gram-negative bacteria. They can penetrate the cell membrane through their hydrophobic region causing hole formation, allowing the leakage of the essential cellular component to seep out or hydrophobic chemicals to pass through the cell. Nevertheless, the

cytotoxicity of AMPs is dose-dependent and will increase with the increase of AMP concentration (Rezaei et al., 2020). Lack of regulated and responsive delivery properties limits the efficacy of such antibacterial agents. (Leekha et al., 2011) Regarding this issue, novel strategies need to be developed to carry and deliver the AMPs to the wound bed in a controlled and sustained manner, protect wounds from resistant bacteria infections and also improve the full-thickness skin wound healing (Rezaei et al., 2020),(Salick et al., 2009).

Autografts, allografts, xenografts, and tissue-engineered skin substitutes have all been used extensively, but there are still substantial issues such as restricted availability, expensive manufacture, variable disease risk, and poor wound healing quality (Choi et al., 2013; Zhang et al., 2022). Recently, the emergence of biological scaffolds derived from decellularized organs or tissues provides an attractive way to overcome these challenges by providing a favorable microenvironment through extracellular matrix (ECM) secreted by resident cells of each tissue and organ to affect cell proliferation, migration, and differentiation(Zhang et al., 2022). Herein, for the reconstruct wounds, the human placenta is offered as a skin substitute. The placenta is a complex organ which is taken after birth and is an excellent source of ECM and bioactive molecules that is configured as a complex 3D structure(Asgari et al., 2021a). In this context, ECM derived from placental tissue with a bioactive component can regulate cellular activity better than any other synthetic biomaterials, making it a good candidate for skin tissue engineering applications(Rameshbabu et al., 2016). The placenta matrix component is similar to the skin and various kinds of growth factors found in the placenta play a role in wound healing. As a result, the compositional and biological characteristics of the placenta led to an ideal environment for wound healing(Choi et al., 2013). Although placental tissue has its AMP, this tissue has weak antibacterial activity against standard strain bacteria and no antibacterial activity against resistant clinical isolates (Asgari et al., 2021b). In the present study, we developed a placental ECM-based sponge loaded with an optimized concentration of cationic AMP (CM11) to fabricate a biological-based skin substitute with strong antibacterial activity against MDR bacteria isolated from burn patients and no cytotoxicity.

2. Materials And Methods

2.1. Study design

The study design is demonstrated in Fig. 1. The placental tissue was collected, decellularized with SDS 1% and Triton 1% and loaded with various concentrations of antimicrobial peptides (AMP). The AMP-loaded decellularized placental tissues were freeze-dried to prepare the AMP-DPS scaffolds. The morphology, mechanical behaviors, *in vitro* and *in vivo* biocompatibility, and antibacterial properties against standard strain and extensively drug-resistant (XDR) clinical isolated bacteria were evaluated to optimize an antibacterial biological-based sponges for management of skin wounds infected with XDR clinical isolates. The human sample collection and *in vivo* biocompatibility assay in the animal model were approved by the ethical committees of Mazandaran University of Medical Sciences and Bushehr University of Medical Sciences, with approval IDs of "IR.MAZUMS.REC.1400.9010" and "IR.BPUMS.REC.1399.122," respectively.

2.1. Placental collection and decellularization

The infectious diseases-free human placentas were received from the consenting mothers after their cesarean section deliveries. The human tissue collection was performed according to the World Medical Association Declaration of Helsinki. The tissue was decellularized using an optimized decellularization technique that is detailed in our previously published work. (Asgari et al., 2021b).

In brief, the tissue was washed several times with sterile distilled water to remove a blood clot. The umbilical cord and chorion/amniotic membrane was carefully removed. The tissue was homogenized on ice, and denuded using 0.5% sodium dodecyl sulfate (SDS, Sigma-Aldrich, MO, USA)) and 0.5% Triton™ X-100 (Sigma-Aldrich, MO, USA), and washed several times with phosphate-buffered saline (PBS; Sigma-Aldrich, MO, USA). Finally, the samples were centrifuged to remove excess PBS.

2.2. Decellularization characterizations

2.2.1. Histological staining

The decellularized placental tissue was stained with hematoxylin and eosin (H&E) to confirm the removal of the cells from the tissue after decellularization. For this purpose, the tissue was fixed with formalin (10%) for 72 h at 4 ℃ and dehydrated through the graded alcohol solution (10%, 30%, 50%, 70%, 96%, and 100%). The dehydrated tissue was embedded in paraffin, and sliced by a microtome (Thermo Fisher Scientific, Massachusetts, Waltham, USA) into little pieces of a thickness equal to 5μm. The tissue slides were then stained using H&E and observed under a light microscope (Olympus Corporation, Tokyo, Japan)(Khosrowpour et al., n.d.).

2.2.2. Masson's trichrome

The remained collagen fibers in placental tissue after the decellularization process were observed by Masson’s trichrome (MT) staining. For this purpose, the tissue slides were de-paraffinized, rehydrated, stained with MT, and visualized under a light microscope (Olympus Corporation, Shinjuku, Tokyo, Japan) (Asgari et al., 2021a).

2.2.3. DNA content

The sample's total DNA content was extracted using a QiaAmp mini kit (Qiagen, USA). The DNA content of the samples before and after decellularization was determined by a NanoDrop spectrophotometer (2000C, Thermo Fisher Scientific, USA).

2.3. Antimicrobial peptide synthesis and antibacterial activity

A cationic antimicrobial peptide (WKLFKKILKVL-NH2) was synthesized using p-methyl benzhydryl amine resin in a solid-phase synthesis method. (Moosazadeh Moghaddam et al., 2018b). Minimum Inhibitory (MIC) and Minimum Bactericidal Concentration (MBC) of AMP for standard strain and patients burn

wound-isolated XDR *Acinetobacter baumannii* was determined using microdilution broth method, according to clinical and laboratory standards institute (CLSI) guidelines(Hsueh et al., 2010). MBC was demonstrated as the lowest concentration of AMP with at least 99.9% bactericidal activity. (Moosazadeh Moghaddam et al., 2018b).

2.4. AMP-loaded DPS fabrication

The decellularized placental tissue was loaded with different concentrations of AMP (0, 16 µg/mL, 32 µg/mL, 64µg/mL, coded as DPS, DPS/AMP1, DPS/AMP2 and DPS/AMP3, respectively) dissolved in sterile distilled water with a 1:1 (v/v) ratio of tissue/AMP. The tissue/AMP samples were poured into a 24-well culture plate, kept at -80 ℃ for 24 h, and then freeze-dried using a freeze drier machine (Alpha 1–2 LD plus, Christ, Germany) for 24 h to fabricate DPS/AMPs scaffolds. The scaffolds were stored at -20°C until they were used.

2.5. AMP-DPS characterizations

2.5.1. Mechanical property

The mechanical behavior of DPS/AMP scaffolds was assessed using a universal testing machine (Hct400/25, Zwick/Roell) equipped with a 100 N load cell and a crosshead loading rate of 5 $mm.min^{-1}$. The scaffolds had a diameter of 4 mm, and a height length of 8 mm. The strain-strain curves were measured and examined to estimate the tensile strength and Young's modulus (Farshi et al., 2022).

2.5.2. Morphology under SEM

A scanning electron microscope (SEM, AIS2100; Seron Technology, Gyeonggi-do, South Korea) was used to examine the microstructure morphology of DPS/AMP scaffolds. The scaffolds were sputtered coated with gold and then observed under an SEM at a 15 kV acceleration voltage (Gholipourmalekabadi et al., 2019)

2.5.3. In vitro cytobiocompatibility

In vitro cytobiocompatibility of the DPS loaded with different concentrations of AMPs for mesenchymal stem cells derived from human adipose tissue (hAD-MSCs) was examined by MTT assay, cell/scaffold morphology under SEM, H&E, and DAPI staining.

2.5.3.1. hAD-MSCs extraction and characterization

Human adipose tissue-derived mesenchymal stem cells (hAD-MSCs) were extracted from human adipose tissue from patients undergoing elective liposuction surgery using a method described in our prior published publication (Gholipourmalekabadi et al., 2016). The isolated cells were characterized by their adherence to the culture plate plastic surface and their spindle morphology under a light microscope. The phenotype of the isolated cells was further characterized by flow cytometry for the expression of CD90 and CD105 surface markers(Hamidabadi et al., 2021).

2.5.3.2. Morphology of hAD-MSCs-DPS/AMP under SEM

The morphology of hAD-MSCs cultured on the DPSs loaded with different concentrations of AMPs was examined under SEM. For this purpose, 3×10^4 hAD-MSCs were cultured on the scaffolds. The cell-scaffold constructs were incubated at 37 ºC for 72h in a standard cell culture incubator. The cells/scaffold constructs were fixed with 2.5% glutaraldehyde and treated with osmium tetroxide (Sigma-Aldrich, MO, USA) for 2h, dehydrated through a graded series of ethanol (10%, 30%, 50%, 70%, 96%, and 100%), sputter coated with gold at room temperature and monitored using SEM (AIS2100; Seron Technology, South Korea) at an acceleration voltage of 20 kV. (Gholipourmalekabadi et al., 2019)

2.5.3.3. H&E

The hAD-MSCs-scaffolds constructs after 7 days of cell culture incubation were fixed with 10% formalin for 72 h at 4 °C, dehydrated through the graded alcohol solution (10%, 30%, 50%, 70%, 96%, and 100%). The samples were paraffin-embedded, and sliced by a microtome (Thermo Fisher Scientific, Waltham, Massachusetts, USA) into 5µm thickness. The H&E-stained slides were observed using a light microscope (Olympus Corporation, Shinjuku, Tokyo, Japan).

2.5.3.4. Cell viability

For the cell metabolic activity assessment, 3 10^3 cells were seeded in a 96-well plate for 24h, then exposed with DPS/AMP scaffolds for 1, 3, and 7 days. After each prescribed time interval, the MTT colorimetric assay was used to evaluate the cell viability as described in our previously published method with minor modifications (Simorgh et al., 2021). Briefly, the cells were treated with the tetrazolium (MTT, Sigma-Aldrich, MO, USA) for 2 h in a cell culture incubator. The cells were then exposed with dimethyl sulfoxide (DMSO, Sigma-Aldrich, MO, USA) for 15 min in a dark chamber and optical density (OD) was determined using an enzyme-linked immunosorbent assay (ELISA) reader at a wavelength of 590 nm with a reference filter of 620 nm. As a control, the cells with no scaffold had 10 % cell viability. The cell viability in percentage was calculated using the following formula (Eq. 1):

$$\text{Cell viability (\%)} = \frac{\text{OD of experiments} - \text{Average OD of negative controls}}{\text{Average OD of positive control}} \times 100 \quad \text{(Eq1)}$$

2.5.4. In vivo biocompatibility

To evaluate the *in vivo* biocompatibility of the scaffolds, the scaffolds with different contents of AMPs were subcutaneously implanted into NMRI male mouse. The detail of the surgery is presented in a study conducted by Yazdanpanah *et al*(Yazdanpanah et al., 2022). In brief, after anesthetization of mice (6–8 weeks, 30 g) by intra-peritoneal injection of 0.01 mg/kg xylazine and 0.1 mg/kg ketamine (both from Anesketin, Heusden–Zolder, Belgium), their back was shaved, opened, and the sterilized scaffolds (8 mm in diameter) were placed subcutaneously and stitched with a silk thread (Supasil 0.1, Supa, Iran). The animals were housed in individuals cages and standard conditions of 25°C and a 12-h cycle of light and

darkness. At day 7 post-implantation, animals were sacrificed by CO_2 asphyxiation, and the implanted area was collected and prepared for H&E staining as previously mentioned. The H&E-stained slides were examined under light microscope (Olympus Corporation, Shinjuku, Tokyo, Japan) to explore body immune system reaction evidences.

2.5.5. Antibacterial activity

2.5.5.1. Disk diffusion assay

Antibacterial activity of the scaffolds with different AMP concentrations against *A. baumannii* (ATCC 19606 standard strain and XDR clinical isolates) was examined using the disk diffusion method, in accordance with the clinical and laboratory standards institute (CLSI) guidelines(Hsueh et al., 2010). Briefly stated, a 0.5 McFarland (1.5×10^8 CFU/mL) suspension of each strain was made and cultured on Mueller-Hinton agar (MHA) plates using a sterile swab. The sterilized scaffolds (disks with 5 mm in diameter) were placed in the middle of the plates and incubated at 37°C in a bacterial culture incubator. The bacterial growth inhibition zone surrounding the disks after 24 h incubation was measured using a ruler and compared between the scaffolds.

2.5.5.1. SEM

For taking micrographs from the ATCC standard strain and XDR clinical isolates *A. baumannii* grown on the scaffolds, a 100 µL of 0.5 McFarland resistant bacteria was seeded on the DPS/AMP scaffolds and incubated at 37°C for 2h (Rezaei et al., 2020). The bacteria-scaffold constructs were then gently rinsed with PBS, fixed with 2.5% glutaraldehyde, stained with osmium tetroxide (Sigma-Aldrich, MO, USA) for 2h, dehydrated through a graded series of alcohol, coated with gold by sputter coating, and viewed under SEM (AIS2100; Seron Technology, South Korea) at an acceleration voltage of 15 kV. (Gholipourmalekabadi et al., 2019)

2.6. Statistical analysis

Analysis of data was done by the GraphPad Prism v8.0.2.263 software using one-way ANOVA or independent samples t-test, where appropriate. The data were reported as mean ± SD. A $P \leq 0.05$ was considered as the level of significance

3. Results

3.1. Decellularization characterizations

The placental tissue before and after decellularization process were subjected to histological evaluations to verify the successful removal of the cells or cellular fragments after decellularization (Fig. 2). The H&E and DAPI staining (Fig. 2A) as well as DNA content assay (Fig. 2B) confirmed successful removal of the cells after decellularization. MT staining demonstrated the presence of collagen fiber after

decellularization. The porous structure of DPS with an interconnected network was observed under SEM microscope (Fig. 2A).

3.2. Antimicrobial peptide synthesis and antibacterial activity

The MIC and MBC values of AMP for ATCC standard strain *A. baumannii* was ≥ 4 μg.mL^{-1} and ≥ 8 μg.mL^{-1}, respectively, while XDR *A. baumannii* showed remarkably higher resistance to AMP with MIC and MBC values of ≥ 32 μg.mL^{-1} and ≥ 32 μg.mL^{-1}, respectively. The MIC and MBC data are shown in Table 1.

Table 1
MIC and MBC of AMP for standard strain and XDR *A. baumannii.*

	AMP	
Strains	**MIC (μg/mL)**	**MBC (μg/mL)**
Acinetobacter baumannii ATCC	4	8
Acinetobacter baumannii XDR	16	16

3.3. AMP-DPS characterizations

3.3.1. Mechanical property

The effect of different concentrations of AMPs on DPS mechanical properties was conducted by tensile strength assay (Fig. 3 and Table 2). The mechanical properties such as elongation at break, tensile strength, and Young's modulus, were evaluated and compared to the DPS group as a control sample. As shown in Fig. 3, the addition AMP didn't affect the mechanical properties of DPS. The detail of mechanical properties is listed in **Table 3**.

Table 2
Tensile mechanical properties (Young's modulus, Tensile strength, and elongation at break for all tested samples)

Group	Young's modulus (MPa)	Tensile strength (MPa)	Elongation at break (%)
DPS	3.0	0.015	1.00
DPS/AMP1	2.6	0.01	1.45
DPS/AMP2	2.5	0.016	1.47
DPS/AMP3	2.3	0.016	1.48

3.3.2. SEM morphology

The SEM images of the scaffolds indicated a uniform, porous and interconnected morphology. No changes in scaffold microstructure were found after adding AMPs. (Fig. 4).

3.3.3. In vitro cytobiocompatibility

3.3.3.1. hAD-MSCs isolation and characterization

The isolated cells displayed spindle and fibroblast-like morphology under a light microscope (Fig. 5A). Flow cytometry revealed that more than 80% of the isolated cells expressed CD90 and CD105 on their surface. (Fig. 5B).

3.3.3.2. SEM

The morphology of the hAD-MSCs grown on DPS/AMP scaffolds was viewed using SEM and is shown in Fig. 6A. The cells were displayed with elongated shape and complete stretching morphology, indicating their cytobiocompatibility and tendency to scaffolds.

3.3.3.3. H&E

The micrographs taken from H&E-stained slides of the scaffold-seeded samples are shown in Fig. 6B. The cells were well penetrated into all the scaffolds and grown within the matrix of placenta.

3.3.3.4. Cell viability

The MTT result showed that the scaffolds without or loaded with various concentrations of AMP did not change the viability of hAD-MSCs during 1, 3 and 7 days cell culture incubation time (Fig. 6C) when compared to the control, which is considered to have 100% cell viability.

3.3.4. In vivo biocompatibility

The subcutaneous implantation of the DPS/AMPs and histological evaluations of the implanted site at day 7 post-implantation revealed no signs of severe acute inflammatory reaction and graft rejection (Fig. 7).

3.3.5. Antibacterial behaviors

3.3.5.1. Disk Diffusion

The bacterial growth inhibition zones around the scaffold disks are shown in Fig. 8A. According to results obtained from the disk diffusion assay, DPS showed no bacterial activity against both standard and XDR bacteria. All the AMP-loaded scaffolds (DPS/AMP1, DPS/AMP2, AND DPS/AMP3) inhibited growth of ATCC bacteria and formed growth inhibition zone, while only DPS/AMP2 and DPS/AMP3 had antibacterial activity against XDR clinical isolates. Disk diffusion data revealed that DPS/AMPs have dose-dependent antibacterial activity against ATCC and XDR bacteria.

3.3.5.2. SEM

The attached and grown bacteria on DPS/AMP scaffolds under SEM are shown in Fig. 8B. As can be seen, the number of bacteria remarkably decreased with the increase of AMP concentration within the construct. The DPS/AMP3 showed a very strong antibacterial activity and caused a considerable decrease in bacteria during 2h exposure.

4. Discussion

The aim of this study was to engineer a decellularized placental sponge loaded with an optimized concentration of AMP with strong antibacterial activity against XDR clinical isolates and standard strain bacteria (ATCC), and excellent biomechanical and biological properties. Drug resistance is currently one of the most pressing issues confronting the medical community(Fjell et al., 2012). Thus, AMPs are considered as potential alternatives because of their wide range antimicrobial activities against infections. These peptides, as host defense peptides, showed the therapeutic potential to wound healing and they exert the anti-infection activity by modulating the immune responses(Miao et al., 2021). Different factors effect on damaging property of AMP including charge, amphipathicity, hydrophobicity and propensity of peptides to form barrels. The difference in membrane lipid compositions and membrane hydrophobicity also affect the sensitivity of eukaryotic cells to AMP in a dose-dependent manner(Yu et al., 2018). Despite the therapeutic potentials of AMPs in skin wound healing model, when AMPs are applied topically, their activity is significantly reduced due to their vulnerability to wound-related situations (alkaline PH and proteolysis) and environmental variables (oxidation, photolysis, and hydrolysis)(Thapa et al., 2020). As a result, a new strategy is needed to develop an effective sustained delivery system with antibacterial activity. The use of decellularized tissue derived-ECM components are considered as an excellent carrier for these peptides. Due to similarity of the placenta matrix component to the skin, the human placenta is offered as a dermal substitute for the full thickness wound healing(Choi et al., 2013; Werner and Grose, 2003). Furthermore, the ECM and bioactive component have

the potential to provide an appropriate environment for wound healing(Benders et al., 2013). In this way, the biologic scaffold was fabricated through the decellularization. Decellularization of placental tissue was conducted using an optimized protocol that has been previously published (Asgari et al., 2021a). SDS (0.5%) and Triton X-100 (0.5%) was used to remove the cellular component. The primary signs of cell removal were confirmed by histological analysis. The result included the DNA quantity less than 50 ng/mg. The absence of detectable cell nuclei was showed with DAPI staining. To fabricate an effective drug delivery system with optimal antibacterial activity and no cytotoxicity, three different concentrations of AMP were loaded into a DPS scaffold to optimize the antibacterial property of the AMP-loaded DPS against ATCC and XDR clinical isolates. The mechanical characteristic of the scaffolds is believed to be an important consideration when dealing with skin tissue engineering(Sander et al., 2014). In this context, the tensile strength, elongation at break, and young modulus, of DPS loaded-AMP were slightly higher than DPS, but the difference was not significant. The different concentrations of AMP didn't affect the mechanical properties of the scaffold. The SEM of both DPS and DPS loaded-AMP showed the interconnected architecture which along with its suitable porosity facilitates cell penetration deep into the scaffold. The AMPs showed to have cytotoxicity effects on eukaryote cells in a dose-dependent manner(Moosazadeh Moghaddam et al., 2018a). So, it is worthy to find an optimal concentration of AMPs in scaffolds in order to achieve a strong antibacterial activity against bacteria of target and high cytocompatibility.

The effects of DPS and DPS loaded with different concentrations of AMPs were determined by exposure of scaffolds to hAD-MSCs. The result showed that the DPS and different concentrations of AMP didn't affect the cell viability during 7 days of incubation time. The hAD-MSC seeded on a placental scaffold by 3D dynamic cell culture promoted cell growth. The SEM images of the cell-DPS constructs confirmed that hAD-MSCs cells successfully integrated and infiltrated into scaffolds. The DPS also supported the cell-friendly property and hence proved to be non-cytotoxic *in vitro.* The *in vivo* biocompatibility of the DPS and DPS/AMPs scaffolds was determined by subcutaneous implantation in an animal model. At day 7 post-implantation, a histological study of the subcutaneously implanted scaffolds demonstrated no severe graft rejection (lack of inflammation), and there was no growth of a fibrous layer surrounding the scaffolds. Overall, it was shown that the implanted DPS were biocompatible *in vivo* by the lack of any negative immunological response in host animals.

Based on the literature, cytotoxicity of AMP was dependent on the AMP type and sequence, and its concentration. In a study, it was shown that loading 50 to 500 µg/mL AMP into a PLGA microsphere had no cytotoxicity for cells (He et al., 2020). In our previous study, we applied various concentrations of CM11 cationic peptide (8, 16, 32 µg/mL) into the silk fibroin sponge to fabricate an antibacterial wound dressing. The scaffold loaded with higher concentrations of AMP (32 µg/ml) showed toxicity for fibroblast cells, while lower AMP concentration was cytobiocompatible (Chizari et al., 2022).

The potential antimicrobial activity of the DPS and DPS loaded with three different concentrations of AMPs was evaluated by disk diffusion assay and SEM. In this study, we used CM11 as our AMP source. The N-terminal domain residues of cecropin a (2–8 residues) and the hydrophobic C–terminal domain

residues of melittin (6–9 residues) combined to form the hybrid peptide known as CM11. CM11 possess strong antibacterial properties against various gram-negative and gram-positive bacteria(Amani et al., 2015). According to the studies, the cationic characteristics of AMP, which are imparted by positively charged lysine or arginine residues, are crucial for their effectiveness. Cationic AMPs bind to bacterial membrane, degrade macromolecules like enzymes and DNA/RNA in the cells, and thereby kill bacteria (Greco et al., 2020). In our previous research, we compared the antibacterial activity of CM11 with silver bioactive glass (AgBG). According to our findings, the MIC of CM11 peptide and 1% AgBG for standard strains bacteria was 8 µg/ml and 1 mg/ml, respectively. MBC of peptide and 1% AgBG were 8 µg/mL and 2 mg/mL, respectively, for the same bacteria(Moosazadeh Moghaddam et al., 2018a). There are some literatures about the antibacterial efficacy of CM11 against MDR strains of a variety range of pathogenic bacteria including *Staphylococcus aureus, Vibrio cholerae, Acinetobacter baumannii, Pseudomonas aeruginosa, Escherichia coli, Salmonella typhimurium, Klebsiella pneumonia, and Brucella melitensis*, (Azad et al., 2017; Moghaddam et al., 2014, 2012; Moosazadeh Moghaddam et al., 2018a). Our antibacterial assays confirmed the antibacterial activity of DPS/AMPs against ATCC and XDR bacteria in a dose-dependent manner, as the bacterial growth inhibition zone around the scaffold disks increased with the increase of AMP concentration. In our previous study, we showed that DPS alone had antibacterial activity against standard strains of *S. aureus* (ATCC 25923) and *E. coli* (ATCC 25922) and, but no detectable antibacterial activity was observed against *P. aeruginosa* standard strain (PAO1) and MDR clinical isolates of *S. aureus* (ATCC 25923) and *E. coli* and *P. aeruginosa* (Asgari et al., 2021b). The current study revealed no antibacterial activity of DPS alone against *A. baumannii* ATCC 19606 standard strain and XDR clinical isolates, while all the DPS/AMPs constructs showed bacterial inhibition against *A. baumannii* ATCC 19606 standard strain. The disk diffusion assay also demonstrated that only DPS/AMP2 and DPS/AMP3 had antibacterial activity against clinical isolates of XDR *A. baumannii*. The same results of the antibacterial activity of DPS and DPS/AMPs were obtained in SEM antibacterial assay. A clear decrease in bacterial number attached to the scaffold was observed with the increase of AMP concentration in DPS/AMP scaffolds.

Various studies showed the dose-dependent antibacterial activity of AMP. Accordingly, Rezaei *et al*., (Rezaei et al., 2020) evaluated the antibacterial activity of different concentrations of AMPs (4, 8, 16 µg/mL) loaded into thermosensitive chitosan (TCTS). As demonstrated, the antibacterial activity with high concentration of AMPs showed greater growth inhibition zone compared with TCTS and lower AMP concentrations.

Our findings suggest DPS/AMP3 with 64µg/mL AMP loaded in the system as a strong antibacterial skin substitute with high antibacterial activity against XDR *A. baumannii* clinical isolates and *in vitro* and *in vivo* biocompatibility.

Conclusion

The current study presents an optimized DPS/AMP3 (64µg/mL) skin substitute with strong antibacterial activity against XDR *A. baumannii* isolated from burn patients. The antibacterial activity of the

DPS/AMPs was dose-dependent, as increased with increasing AMP concentration in the scaffold. The *in vitro* and *in vivo* studies verified the biocompatibility of the DPS/AMP3. As a conclusion, the DPS/AMP3 scaffold is suggested as an excellent antibacterial skin substitute, and now promises to proceed with pre-clinical and clinical investigations.

Declarations

Acknowledgement

This study was funded by a grant from the Mazandaran University of Medical Sciences under grant number (1400.9010), and Bushehr University of Medical Sciences under grant number (1399.122).

Author contribution

MG and MZ conceived and designed the study. HHG, SA, ZK, LB, MNB and ZAA performed the experiments. MG, MZ, HGH, MNB, SA and ZK analyzed the data and interpreted the results. HGH, SA, LM, ZAA, ZK and MMS prepared the manuscript. MG, NPS and MZ reviewed during the manuscript preparation and revised the manuscript.

Conflict of interest

There is no conflict of interest.

References

1. Ahovan, Z.A., Khosravimelal, S., Eftekhari, B.S., Mehrabi, S., Hashemi, A., Eftekhari, S., Milan, P.B., Mobaraki, M., Seifalian, A.M., Gholipourmalekabadi, M., 2020. Thermo-responsive chitosan hydrogel for healing of full-thickness wounds infected with XDR bacteria isolated from burn patients: In vitro and in vivo animal model. Int. J. Biol. Macromol. 164, 4475–4486.
2. Amani, J., A Barjini, K., M Moghaddam, M., Asadi, A., 2015. In vitro synergistic effect of the CM11 antimicrobial peptide in combination with common antibiotics against clinical isolates of six species of multidrug-resistant pathogenic bacteria. Protein Pept. Lett. 22, 940–951.
3. Asgari, F., Asgari, H.R., Najafi, M., Eftekhari, B.S., Vardiani, M., Gholipourmalekabadi, M., Koruji, M., 2021a. Optimization of decellularized human placental macroporous scaffolds for spermatogonial stem cells homing. J. Mater. Sci. Mater. Med. 32, 1–17.
4. Asgari, F., Khosravimelal, S., Koruji, M., Ahovan, Z.A., Shirani, A., Hashemi, A., Hamidabadi, H.G., Chauhan, N.P.S., Moroni, L., Reis, R.L., 2021b. Long-term preservation effects on biological properties of acellular placental sponge patches. Mater. Sci. Eng. C 121, 111814.
5. Azad, Z.M., Moravej, H., Fasihi-Ramandi, M., Masjedian, F., Nazari, R., Mirnejad, R., Moghaddam, M.M., 2017. In vitro synergistic effects of a short cationic peptide and clinically used antibiotics against drug-resistant isolates of Brucella melitensis. J. Med. Microbiol. 66, 919–926.

6. Benders, K.E.M., van Weeren, P.R., Badylak, S.F., Saris, D.B.F., Dhert, W.J.A., Malda, J., 2013. Extracellular matrix scaffolds for cartilage and bone regeneration. Trends Biotechnol. 31, 169–176.
7. Chizari, M., Khosravimelal, S. of an A.P.-L.S.F.B.S. to A. as a W.D.A.I.V.S., Tebyaniyan, H., Moosazadeh Moghaddam, M., Gholipourmalekabadi, M., 2022. Fabrication of an Antimicrobial Peptide-Loaded Silk Fibroin/Gelatin Bilayer Sponge to Apply as a Wound Dressing, An In Vitro Study. Int. J. Pept. Res. Ther. 28, 1–13.
8. Choi, J.S., Kim, J.D., Yoon, H.S., Cho, Y.W., 2013. Full-thickness skin wound healing using human placenta-derived extracellular matrix containing bioactive molecules. Tissue Eng. - Part A 19, 329–339. https://doi.org/10.1089/ten.tea.2011.0738
9. Farshi, P., Salarian, R., Rabiee, M., Alizadeh, S., Gholipourmalekabadi, M., Ahmadi, S., Rabiee, N., 2022. Design, preparation, and characterization of silk fibroin/carboxymethyl cellulose wound dressing for skin tissue regeneration applications. Polym. Eng. Sci.
10. Fjell, C.D., Hiss, J.A., Hancock, R.E.W., Schneider, G., 2012. Designing antimicrobial peptides: form follows function. Nat. Rev. Drug Discov. 11, 37–51.
11. Gholipourmalekabadi, M., Khosravimelal, S., Nokhbedehghan, Z., Sameni, M., Jajarmi, V., Urbanska, A.M., Mirzaei, H., Salimi, M., Chauhan, N.P.S., Mobaraki, M., 2019. Modulation of hypertrophic scar formation using amniotic membrane/electrospun silk fibroin bilayer membrane in a rabbit ear model. ACS Biomater. Sci. Eng. 5, 1487–1496.
12. Gholipourmalekabadi, M., Sameni, M., Radenkovic, D., Mozafari, M., Mossahebi-Mohammadi, M., Seifalian, A., 2016. Decellularized human amniotic membrane: how viable is it as a delivery system for human adipose tissue-derived stromal cells? Cell Prolif. 49, 115–121.
13. Greco, I., Molchanova, N., Holmedal, E., Jenssen, H., Hummel, B.D., Watts, J.L., Håkansson, J., Hansen, P.R., Svenson, J., 2020. Correlation between hemolytic activity, cytotoxicity and systemic in vivo toxicity of synthetic antimicrobial peptides. Sci. Rep. 10, 1–13.
14. Hamidabadi, H.G., Simorgh, S., Kamrava, S.K., Namjoo, Z., Bagher, Z., Bojnordi, M.N., Niapour, A., Mojaverrostami, S., Saeb, M.R., Zarrintaj, P., 2021. Promoting motor functions in a spinal cord injury model of rats using transplantation of differentiated human olfactory stem cells: A step towards future therapy. Behav. Brain Res. 405, 113205.
15. He, Y., Jin, Y., Ying, X., Wu, Q., Yao, S., Li, Y., Liu, H., Ma, G., Wang, X., 2020. Development of an antimicrobial peptide-loaded mineralized collagen bone scaffold for infective bone defect repair. Regen. Biomater. 7, 515–525.
16. Hsueh, P.-R., Ko, W.-C., Wu, J.-J., Lu, J.-J., Wang, F.-D., Wu, H.-Y., Wu, T.-L., Teng, L.-J., 2010. Consensus statement on the adherence to Clinical and Laboratory Standards Institute (CLSI) Antimicrobial Susceptibility Testing Guidelines (CLSI-2010 and CLSI-2010-update) for Enterobacteriaceae in clinical microbiology laboratories in Taiwan. J. Microbiol. Immunol. Infect. 43, 452–455.
17. Khosrowpour, Z., Hashemi, S.M., Mohammadi-Yeganeh, S., Moghtadaei, M., Brouki Milan, P., Moroni, L., Kundu, S.C., Gholipourmalekabadi, M., n.d. Coculture of adipose-derived mesenchymal stem

cells/macrophages on decellularized placental sponge promotes differentiation into the osteogenic lineage. Artif. Organs.

18. Leekha, S., Terrell, C.L., Edson, R.S., 2011. General principles of antimicrobial therapy, in: Mayo Clinic Proceedings. Elsevier, pp. 156–167.
19. Mahlapuu, M., Håkansson, J., Ringstad, L., Björn, C., 2016. Antimicrobial peptides: an emerging category of therapeutic agents. Front. Cell. Infect. Microbiol. 6, 194.
20. Miao, F., Li, Y., Tai, Z., Zhang, Y., Gao, Y., Hu, M., Zhu, Q., 2021. Antimicrobial Peptides: The Promising Therapeutics for Cutaneous Wound Healing. Macromol. Biosci. 21, 2100103.
21. Moghaddam, M.M., Abolhassani, F., Babavalian, H., Mirnejad, R., Azizi Barjini, K., Amani, J., 2012. Comparison of in vitro antibacterial activities of two cationic peptides CM15 and CM11 against five pathogenic bacteria: Pseudomonas aeruginosa, Staphylococcus aureus, Vibrio cholerae, Acinetobacter baumannii, and Escherichia coli. Probiotics Antimicrob. Proteins 4, 133–139.
22. Moghaddam, M.M., Barjini, K.A., Ramandi, M.F., Amani, J., 2014. Investigation of the antibacterial activity of a short cationic peptide against multidrug-resistant Klebsiella pneumoniae and Salmonella typhimurium strains and its cytotoxicity on eukaryotic cells. World J. Microbiol. Biotechnol. 30, 1533–1540.
23. Moosazadeh Moghaddam, M., Eftekhary, M., Erfanimanesh, S., Hashemi, A., Fallah Omrani, V., Farhadihosseinabadi, B., Lasjerdi, Z., Mossahebi-Mohammadi, M., Pal Singh Chauhan, N., Seifalian, A.M., 2018a. Comparison of the antibacterial effects of a short cationic peptide and 1% silver bioactive glass against extensively drug-resistant bacteria, Pseudomonas aeruginosa and Acinetobacter baumannii, isolated from burn patients. Amino Acids 50, 1617–1628.
24. Moosazadeh Moghaddam, M., Eftekhary, M., Erfanimanesh, S., Hashemi, A., Fallah Omrani, V., Farhadihosseinabadi, B., Lasjerdi, Z., Mossahebi-Mohammadi, M., Pal Singh Chauhan, N., Seifalian, A.M., 2018b. Consensus statement on the adherence to Clinical and Laboratory Standards Institute (CLSI) Antimicrobial Susceptibility Testing Guidelines (CLSI-2010 and CLSI-2010-update) for Enterobacteriaceae in clinical microbiology laboratories in Taiwan, J. Amino Acids 50, 1617–1628.
25. Rameshbabu, A.P., Ghosh, P., Subramani, E., Bankoti, K., Kapat, K., Datta, S., Maity, P.P., Subramanian, B., Roy, S., Chaudhury, K., 2016. Investigating the potential of human placenta-derived extracellular matrix sponges coupled with amniotic membrane-derived stem cells for osteochondral tissue engineering. J. Mater. Chem. B 4, 613–625.
26. Rezaei, N., Hamidabadi, H.G., Khosravimelal, S., Zahiri, M., Ahovan, Z.A., Bojnordi, M.N., Eftekhari, B.S., Hashemi, A., Ganji, F., Darabi, S., 2020. Antimicrobial peptides-loaded smart chitosan hydrogel: Release behavior and antibacterial potential against antibiotic resistant clinical isolates. Int. J. Biol. Macromol. 164, 855–862.
27. Salick, D.A., Pochan, D.J., Schneider, J.P., 2009. Design of an Injectable β-Hairpin Peptide Hydrogel That Kills Methicillin-Resistant Staphylococcus aureus. Adv. Mater. 21, 4120–4123.
28. Sander, E.A., Lynch, K.A., Boyce, S.T., 2014. Development of the mechanical properties of engineered skin substitutes after grafting to full-thickness wounds. J. Biomech. Eng. 136, 51008.

29. Simorgh, S., Milan, P.B., Saadatmand, M., Bagher, Z., Gholipourmalekabadi, M., Alizadeh, R., Hivechi, A., Arabpour, Z., Hamidi, M., Delattre, C., 2021. Human olfactory mucosa stem cells delivery using a collagen hydrogel: as a potential Candidate for bone tissue Engineering. Materials (Basel). 14, 3909.
30. Thapa, R.K., Diep, D.B., Tønnesen, H.H., 2020. Topical antimicrobial peptide formulations for wound healing: Current developments and future prospects. Acta Biomater. 103, 52–67.
31. Werner, S., Grose, R., 2003. Regulation of wound healing by growth factors and cytokines. Physiol. Rev. 83, 835–870.
32. Yazdanpanah, A., Madjd, Z., Pezeshki-Modaress, M., Khosrowpour, Z., Farshi, P., Eini, L., Kiani, J., Seifi, M., Kundu, S.C., Ghods, R., 2022. Bioengineering of fibroblast-conditioned polycaprolactone/gelatin electrospun scaffold for skin tissue engineering. Artif. Organs 46, 1040–1054.
33. Yu, G., Baeder, D.Y., Regoes, R.R., Rolff, J., 2018. Predicting drug resistance evolution: insights from antimicrobial peptides and antibiotics. Proc. R. Soc. B Biol. Sci. 285, 20172687.
34. Zhang, X., Chen, X., Hong, H., Hu, R., Liu, J., Liu, C., 2022. Decellularized extracellular matrix scaffolds: recent trends and emerging strategies in tissue engineering. Bioact. Mater. 10, 15–31.

Figures

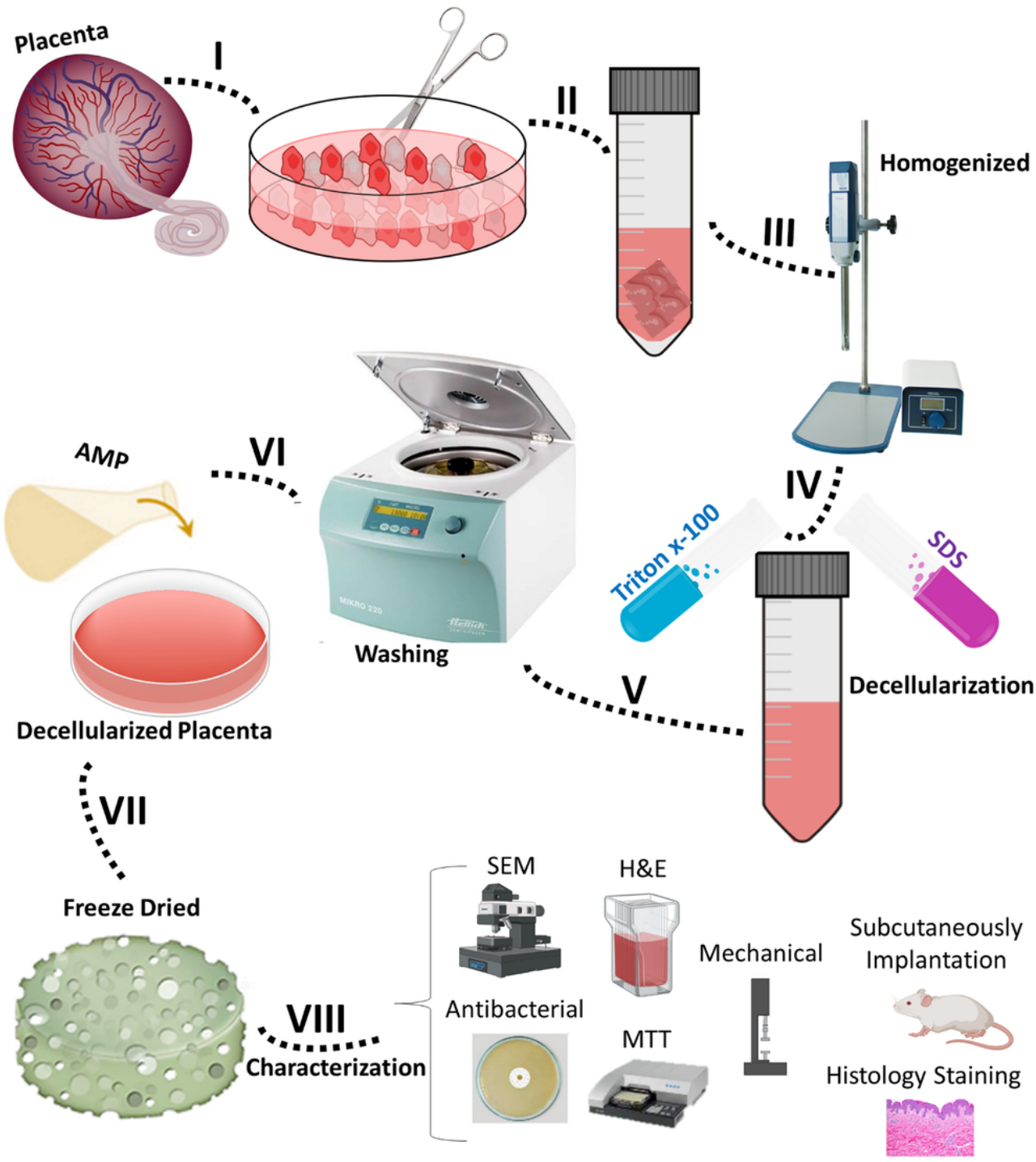

Figure 1

A summary of the present study design. The placental tissues were collected and decellularized. Then, different concentrations of antimicrobial peptides (AMP) are loaded in the decellularized placenta, and finally freeze-dried to fabricate AMP-loaded decellularized placental sponges (AMP-DPS) scaffolds. After the biological and biomechanical properties of the DPS/AMP scaffolds were fully characterized *in vitro* and *in vivo.* Antibacterial assays were used to determine the antibacterial behavior of DPS loaded with

three various concentrations of AMPs to optimize an antibacterial DPS scaffold with biocompatibility and antibacterial activity against resistant clinical isolated bacteria.

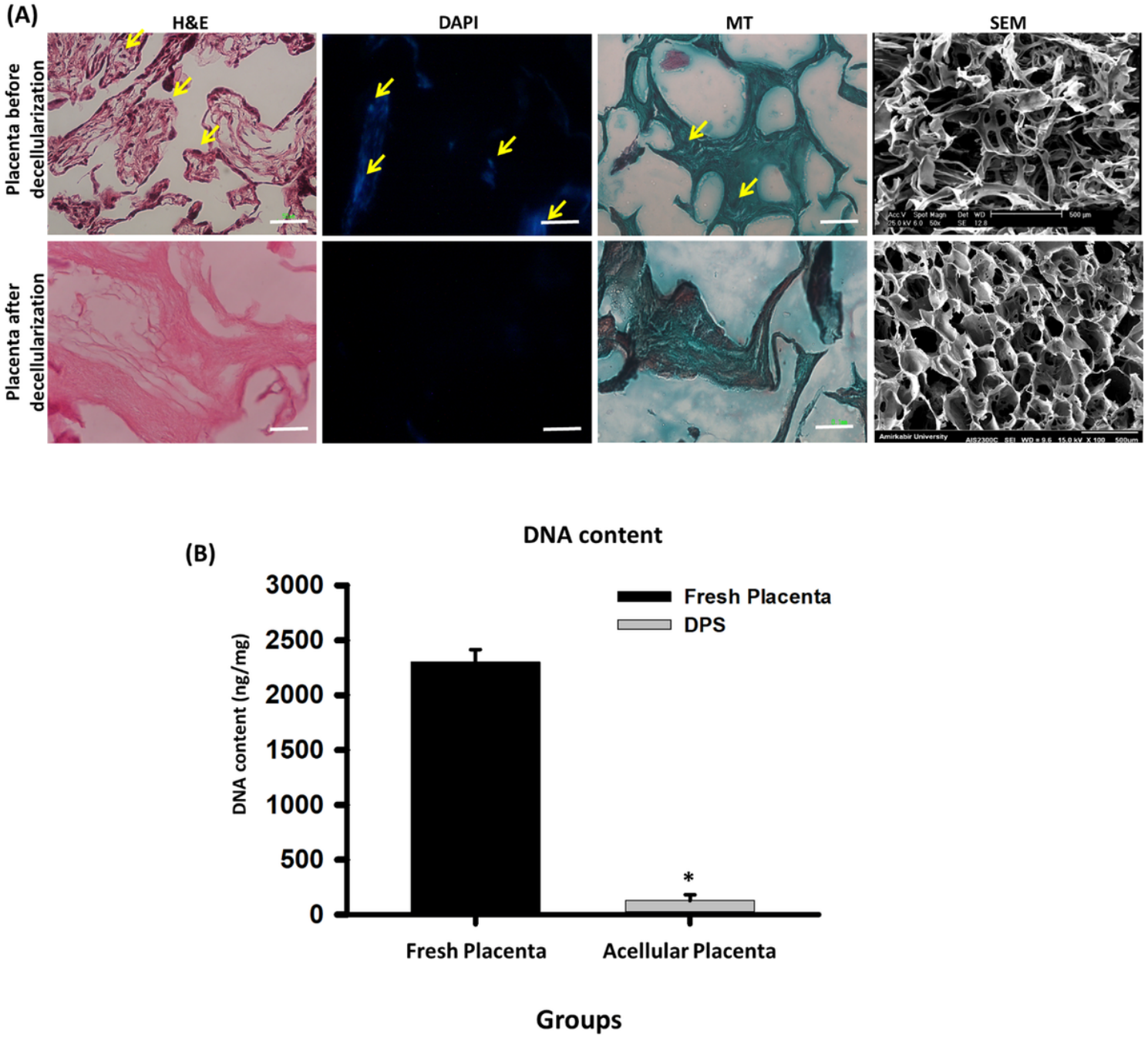

Figure 2

A. H&E staining, DAPI, MT, and SEM evaluations of the placenta before and after decellularization. B. DNA quantification of the fresh placenta and acellular placenta. Yellow arrow point to cells. Scale bar: 50 μm. H&E: hematoxylin and eosin, DAPI: 4, 6-diamidino-2-phenylindole, MT: Masson's trichrome, SEM: scanning electron microscopy. *indicates significant difference (P .05)

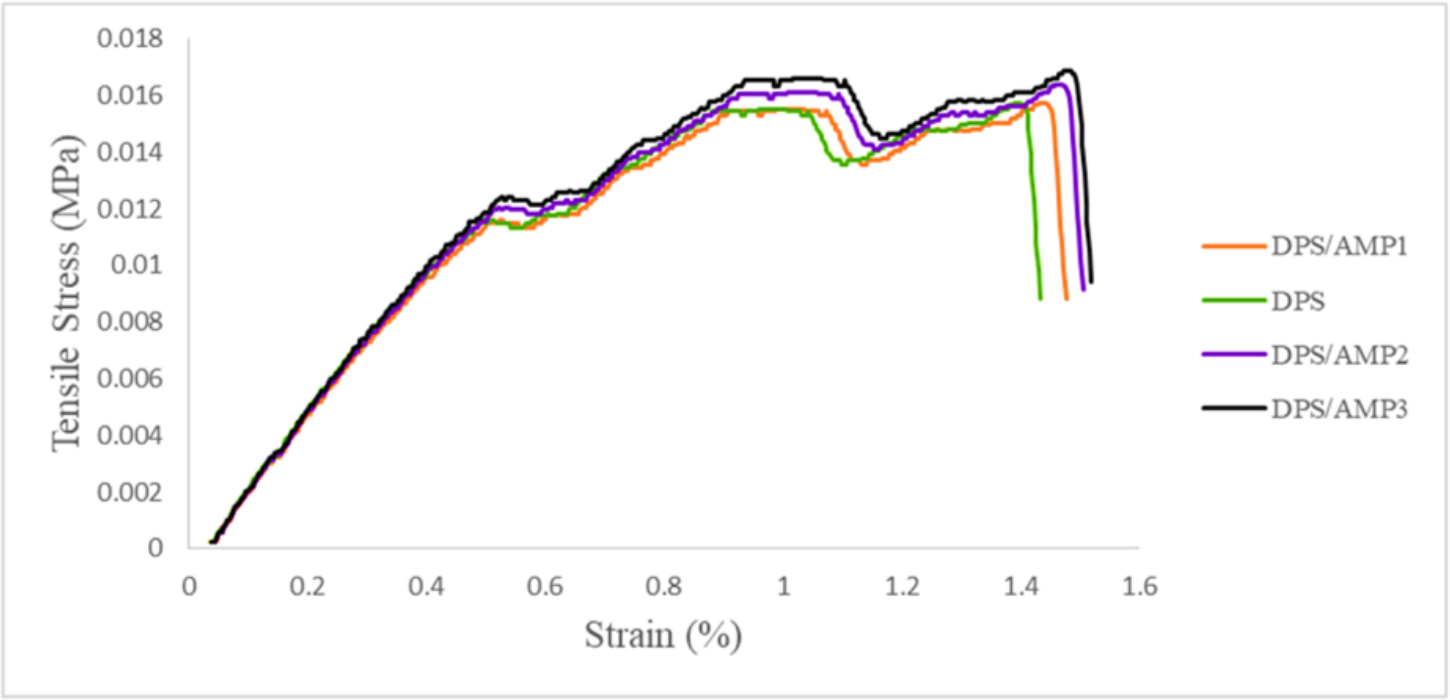

Figure 3

Tensile stress-strain curve of different groups of AMP-loaded DPS.

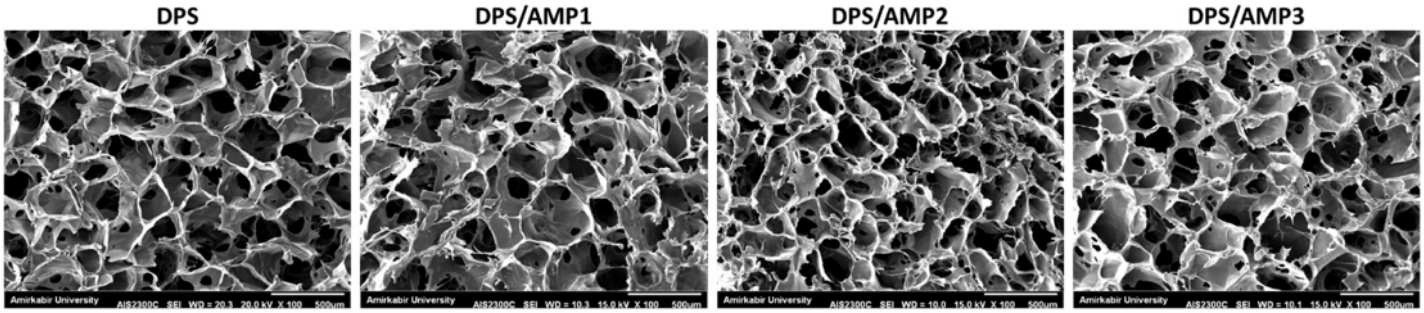

Figure 4

The morphology of DPS and DPS loaded with different concentrations of AMPs (DPS/AMP1, DPS/AMP2 and DPS/AMP3) using scanning electron microscopy (SEM). Scale bar: 100 μm.

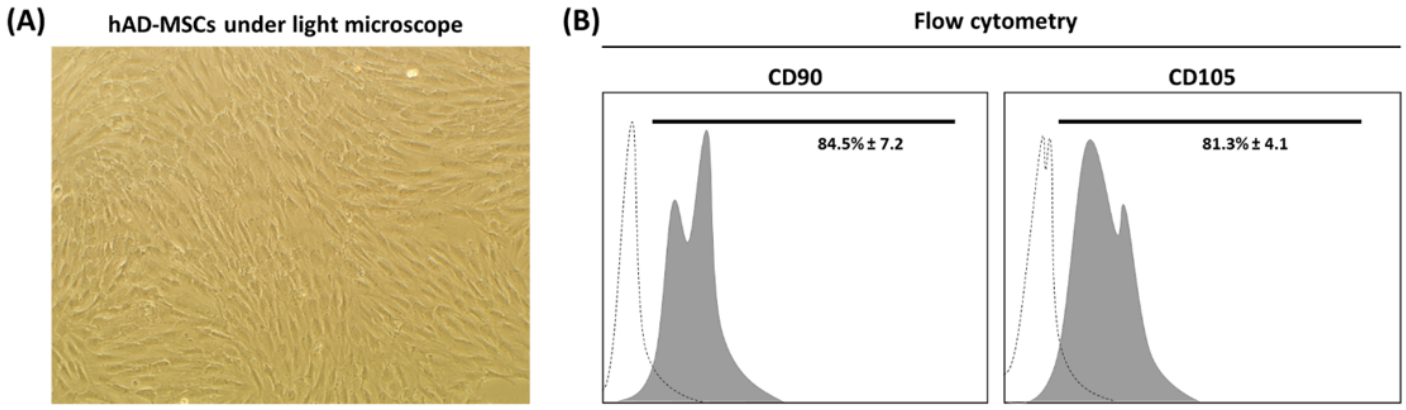

Figure 5

A. Morphological feature of human adipose derived mesenchymal stem cells under light microscopy on day 3 of culture. B. Flow cytometry analysis of the surface molecule markers (CD90 and CD105).

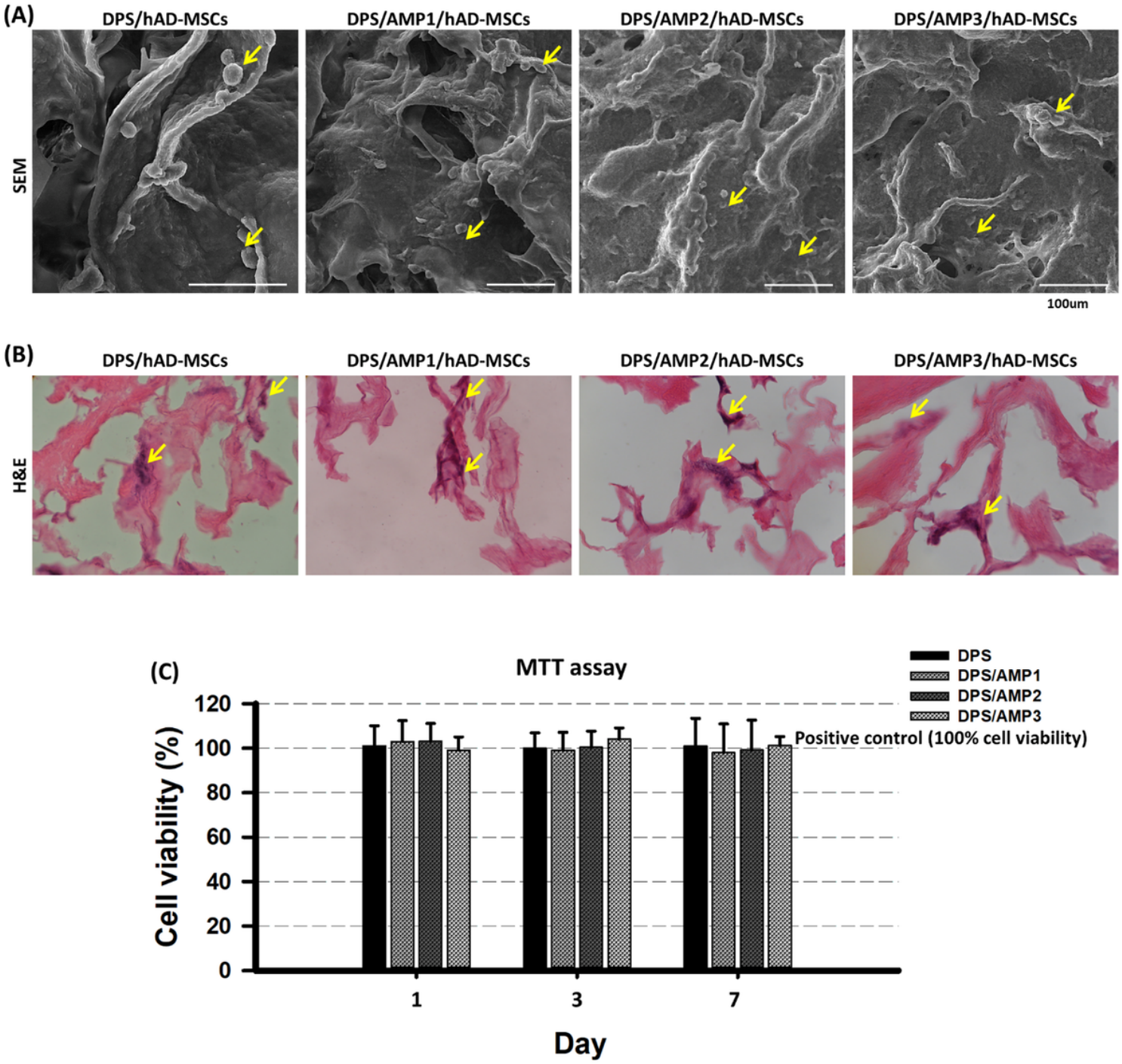

Figure 6

hAD-MSCs-scaffolds interaction. A. SEM micrographs of hAD-MSCs morphology cultured and adhered to the DPS and DPS loaded with different concentrations of AMPs (DPS/AMP1, DPS/AMP2 and DPS/AMP3). B. H&E staining of the scaffolds seeded with hAD-MSCs for 72 h. C. The viability of hAD-MSCs grown on scaffolds after 1, 3, and 7 days of culture. The cells were represented by a yellow arrow.

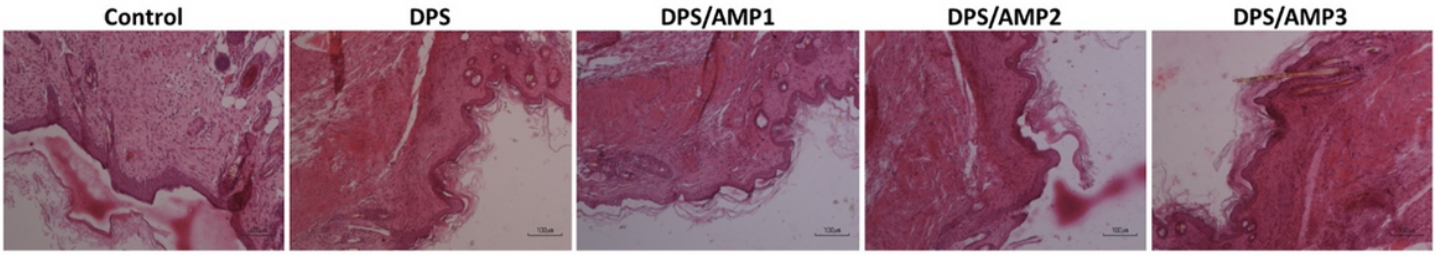

Figure 7

H&E staining of the subcutaneously implanted DPS and DPS/AMP scaffolds during 7 days follow up.

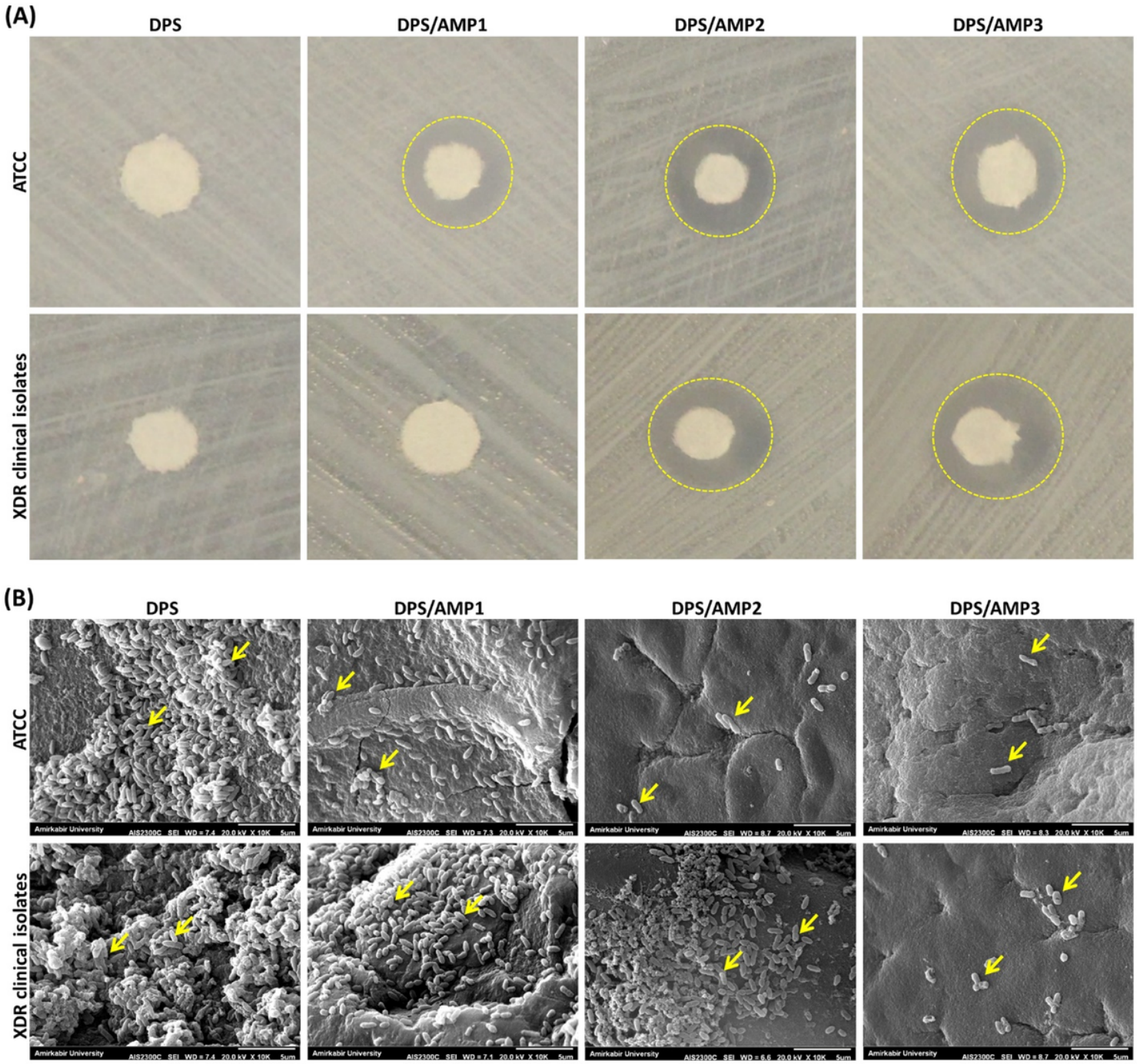

Figure 8

A. Disk diffusion assay for the DPS and DPS/AMP against *A. baumannii* (XDR clinical isolates and ATCC 19606 standard strain). The DPS/AMP3 and DPS/AMP2 demonstrated a growth inhibition zone around ATCC and XDR. The DPS/AMP1 showed a growth inhibition zone around ATCC, whereas no inhibition zone was found for XDR. The DPS showed no bacterial growth inhibition zone for ATCC and XDR. B. SEM images revealed that the growth of standard and XDR strain bacteria on DPS and DPS/AMP. The bacteria growing on the various scaffolds are indicated by yellow arrows. Scale bar: 50μm.